

## NOTES AND CORRESPONDENCE

### Interactions between a Supercell and a Quasi-Stationary Frontal Boundary

DAVID O. BLANCHARD

*NOAA/National Weather Service, Flagstaff, Arizona*

(Manuscript received 25 October 2007, in final form 23 March 2008)

#### ABSTRACT

The case presented here is submitted as an example of a previously undocumented type of interaction between a supercell thunderstorm and a frontal boundary. During the afternoon of 8 June 1995, a supercell thunderstorm formed near a quasi-stationary frontal boundary and then moved northeast across Beaver County in the Oklahoma Panhandle. Its motion took it away from the boundary and deeper into the cool air. As the storm matured and strengthened, a portion of the boundary to the south of the supercell moved northward and briefly became entrained in the low-level circulation of the storm. This northward advance of the boundary was subsequently followed by a southward motion back to near its original location. High-density spatial and temporal observations from the Oklahoma Mesonet and the Verification of the Origins of Rotation in Tornadoes Experiment (VORTEX) Mobile Mesonet are presented to document the northward advance of the boundary into the supercell circulation.

#### 1. Introduction

The Verification of the Origins of Rotation in Tornadoes Experiment (VORTEX; Rasmussen et al. 1994) was conducted in the central and southern plains of Kansas, Oklahoma, and Texas during the spring months of 1994 and 1995. A primary goal of the program was to collect data using multiple platforms that could then be analyzed to test and possibly refute various tornadogenesis hypotheses.

On 8 June 1995, VORTEX scientists collected data on a strong, long-lived supercell. This storm persisted for many hours as it moved from the northern Texas Panhandle into Beaver County in the Oklahoma Panhandle (hereinafter referred to as the Beaver County storm). The supercell storm initiated on a quasi-stationary frontal boundary then moved to the northeast away from the boundary and deeper into the cool air located north of the front. Surface data, however, indicate that a portion of the frontal boundary south of the supercell storm moved northward and became briefly entrained in the low-level circulation of the su-

percell before moving southward back to near its original location.

The interaction between the boundary and the supercell described here depicts an evolution not previously documented in the formal literature. The intent of the work presented here is to document the interaction between the supercell and boundary using the enhanced datasets available during VORTEX. Airborne and ground-based Doppler radar, surface mesonet, mobile mesonet, and mobile upper-air sounding systems allow a detailed examination of the supercell storm, its near-storm environment, and the interaction of the boundary with the supercell.

This interaction is interesting because recent work has suggested that a supercell is more likely to become tornadic if it remains near a surface boundary in which low-level horizontal vorticity associated with the boundary can be tilted into the vertical (Markowski et al. 1998; Rasmussen et al. 2000) or there is enhanced stretching of vertical vorticity along the boundary as described by Maddox et al. (1980). No attempt is made herein to determine why this storm failed to produce a tornado. Such an analysis is beyond the scope of the current study.

A brief description of the various data platforms is given in section 2. The large-scale and near-storm environments are presented in section 3. Section 4 de-

---

*Corresponding author address:* David O. Blanchard, NOAA/National Weather Service, P.O. Box 16057, Belmont, AZ 86015.  
E-mail: david.o.blanchard@noaa.gov

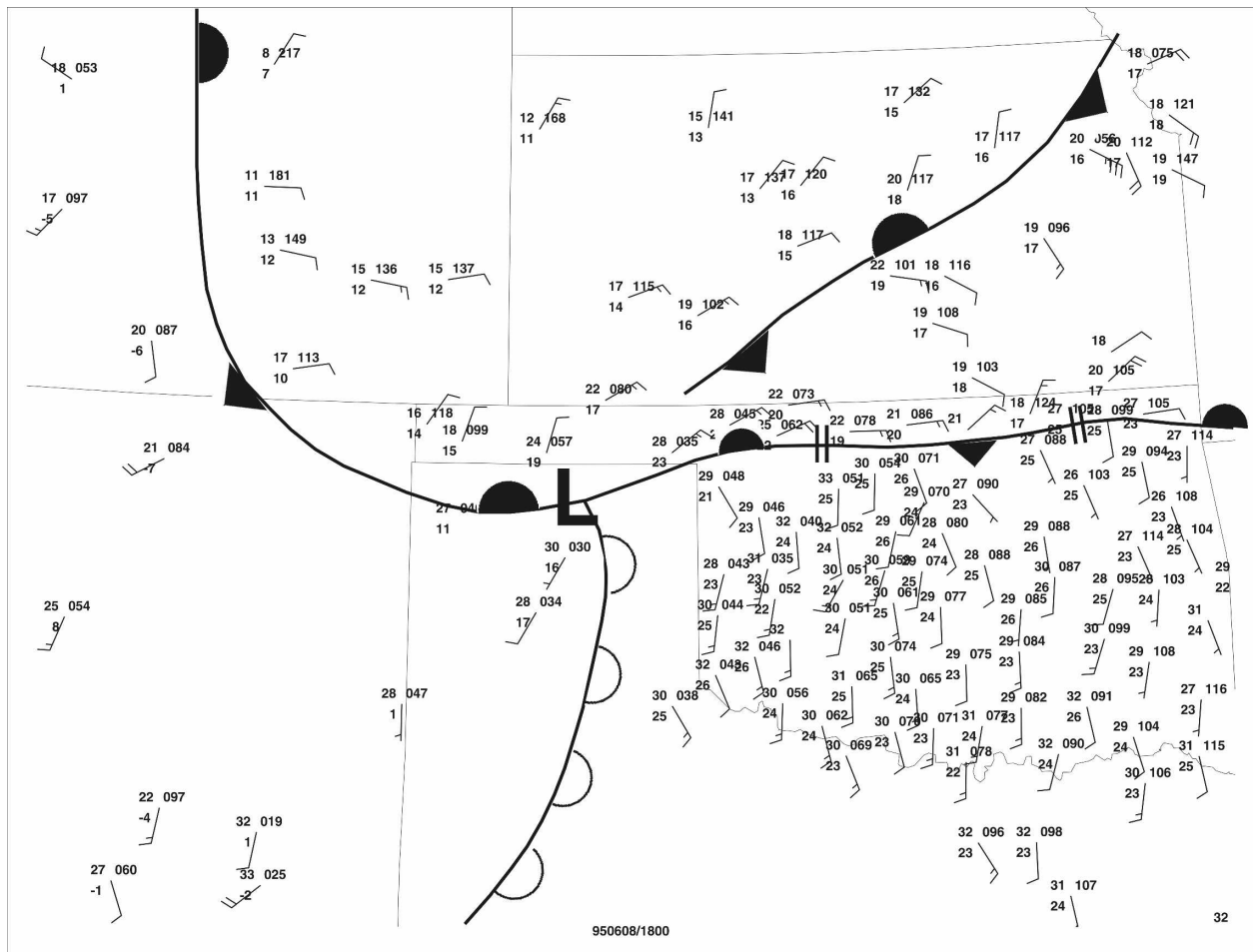


FIG. 1. Surface analysis at 1800 UTC 8 Jun 1995. Station plots include temperature (upper left) and dewpoint (lower left) in degrees Celsius and pressure (upper right) in hectopascals (denoted the standard way, with an implied decimal point before the last digit and an omitted “10” or “9” in front of the value). Wind barbs are in meters per second, with a full barb at  $5 \text{ m s}^{-1}$  and a half barb at  $2.5 \text{ m s}^{-1}$ . Frontal and mesoscale boundaries use the format of Young and Fritsch (1989).

scribes the interaction between the surface boundary and the supercell. A discussion of the current study and how it compares and contrasts with previous similar studies is presented in section 5.

## 2. Data description

Data collected on this day included National Weather Service (NWS) and Federal Aviation Administration surface aviation reports, Oklahoma Mesonet surface reports (Brock et al. 1995), NWS Weather Surveillance Radar-1988 Doppler (WSR-88D) observations, satellite imagery, and upper-air rawinsondes. Additional VORTEX datasets included airborne and mobile Doppler radar, mobile upper-air sounding facilities, and mobile surface mesonets. A few of these datasets are briefly discussed below.

### a. Airborne Doppler radar data

Two aircraft were committed to VORTEX in 1995: the National Oceanic and Atmospheric Administration (NOAA) P-3 and the National Center for Atmospheric Research (NCAR) Electra. The primary mission of the two aircraft was to gather pseudo-dual-Doppler datasets focusing on the evolution of the low-level mesocyclone region of the tornadic storm that the ground intercept teams were investigating.

The NCAR Electra Doppler radar (ELDORA) collected data using two helically scanning antennas mounted in a rotating structure contained within the tail section of the aircraft. The antenna rotated about the aircraft’s longitudinal axis and provided continuous sampling on both sides of the aircraft. The radars transmitted in the X band ( $\sim 3\text{-cm}$  wavelength) and had a circular beamwidth of  $1.8^\circ$ . These scans were close to

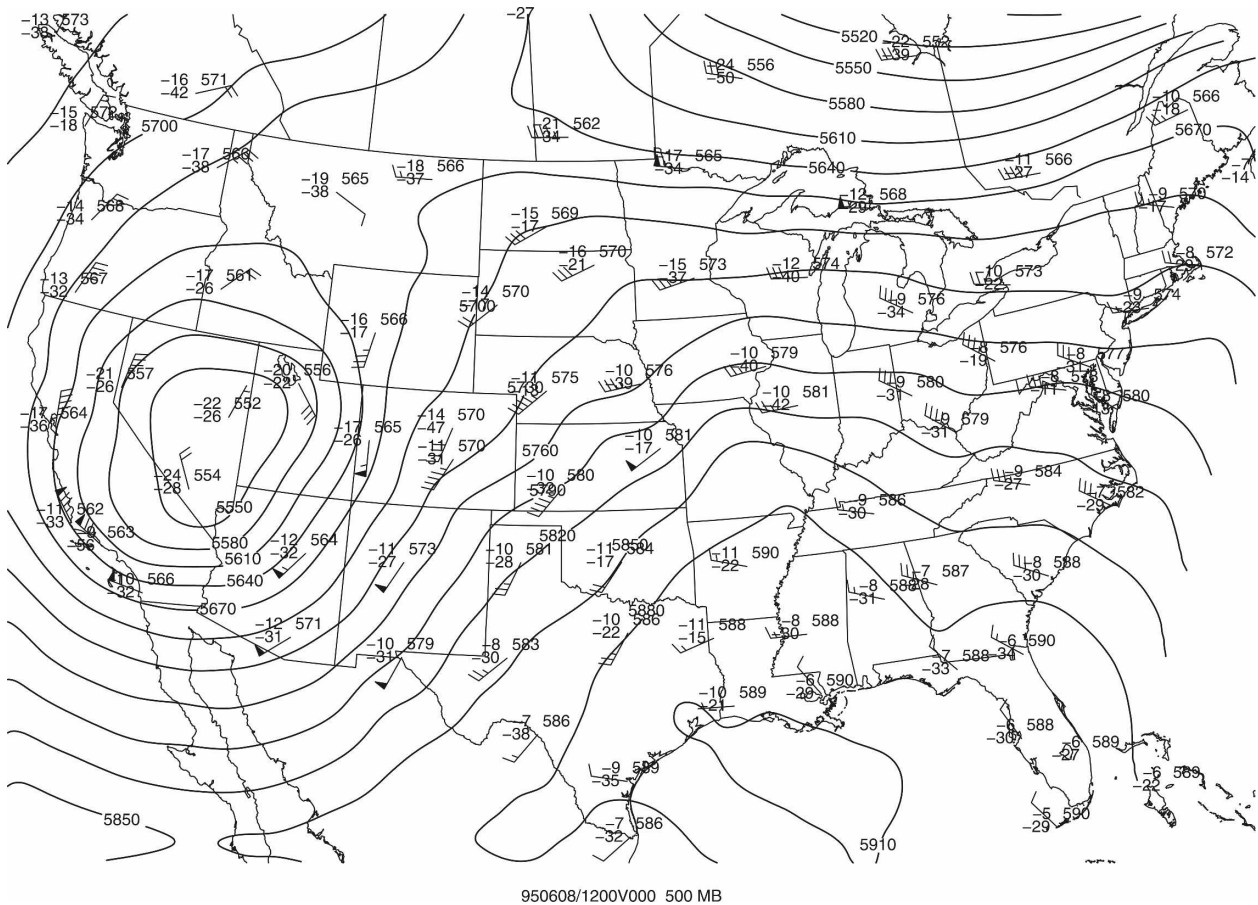


FIG. 2. Analysis of the 500-hPa surface at 1200 UTC 8 Jun 1995. Height contours are drawn every 30 m. Wind bars are in meters per second, with a flag denoting  $25 \text{ m s}^{-1}$ , a full barb denoting  $5 \text{ m s}^{-1}$ , and a half barb denoting  $2.5 \text{ m s}^{-1}$ .

being vertical cross sections or range–height indicators (RHIs) but owing to the forward motion of the aircraft were helical. Additional details on the operation of the ELDORA and the process of obtaining dual-Doppler winds can be found in both Wakimoto et al. (1996) and Hildebrand et al. (1996).

No radar data were available from the NOAA P-3 during the period of investigation of this storm because of hardware problems.

### b. Doppler on Wheels

Mobile, ground-based, Doppler radar data were made available by the X-band Doppler on Wheels (DOW; Wurman et al. 1997). The DOW was mounted on a truck for portability and was designed to deploy quickly in severe weather environments, conduct volumetric scans at rapid update rates, and display Doppler velocity and reflectivity data in real time for coordination and safety purposes.

The DOW was first employed in the final weeks of

VORTEX, thus it was only partially functional and incomplete in many respects. Despite the problems inherent in a prototype system, the data from DOW were still useful since the analysis presented here focuses primarily on the reflectivity field to describe the supercell structure.

### c. Mobile Mesonet data

One of the more unique data collection systems developed for and deployed during VORTEX was the Mobile Mesonet (MM; Rasmussen et al. 1994; Straka et al. 1996). Storm-scale surface data were collected by placing an instrument package on each vehicle and recording vehicle position, velocity, and meteorological variables (e.g., temperature, humidity, pressure, wind direction, and speed) approximately every 2 s. Vehicle velocity, determined from global positioning system readings, was subtracted from vehicle winds to obtain ground-relative winds.

The MM 2-s data were averaged over 12-s intervals

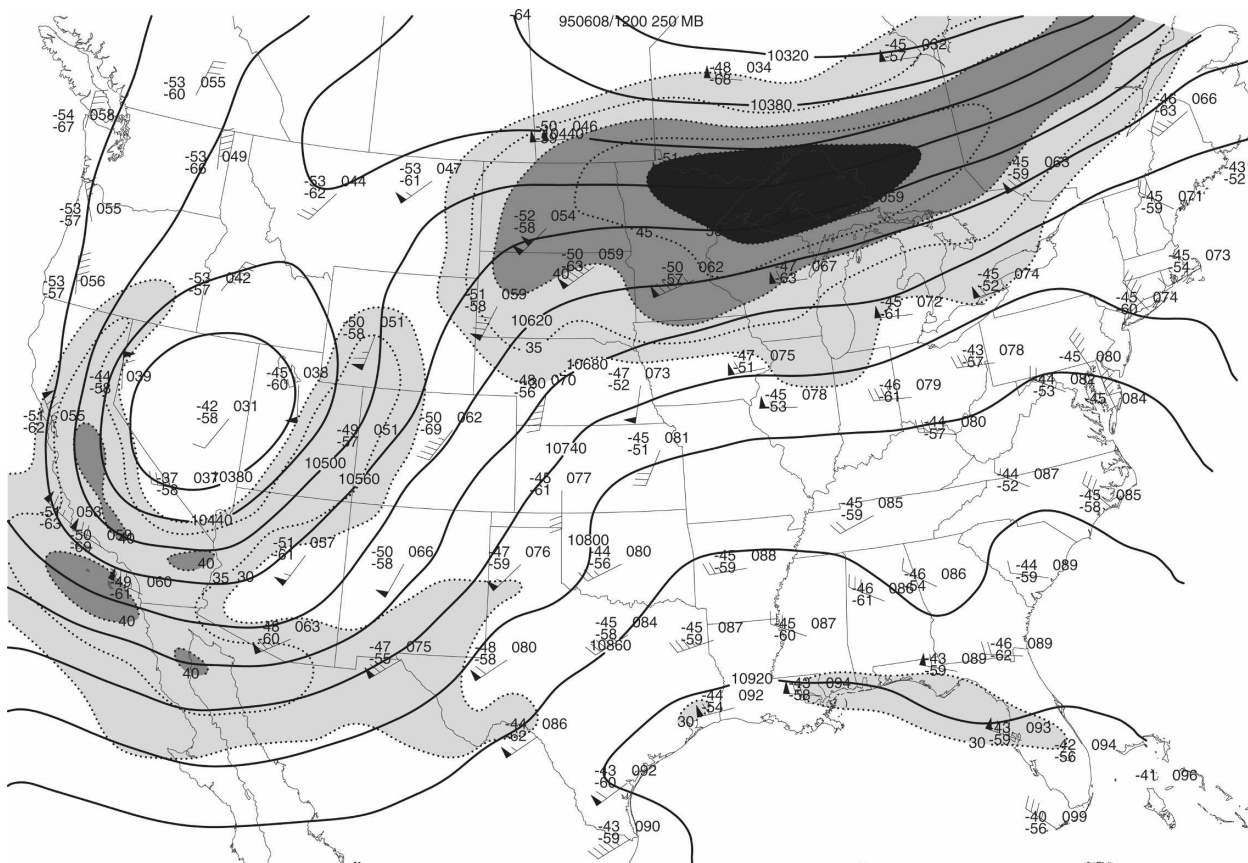


FIG. 3. Analysis of the 250-hPa surface at 1200 UTC 8 Jun 1995. Height contours (solid lines) are drawn every 60 m. Wind barbs are in meters per second, with a flag denoting  $25 \text{ m s}^{-1}$ , a full barb denoting  $5 \text{ m s}^{-1}$ , and a half barb denoting  $2.5 \text{ m s}^{-1}$ . Isotachs (dashed lines) are drawn every  $5 \text{ m s}^{-1}$ , starting at  $30 \text{ m s}^{-1}$ . The various shades of gray denote wind speeds in excess of 30, 40, and  $50 \text{ m s}^{-1}$ .

and the results were plotted relative to the radar echoes using time-to-space conversion. For the work reported here, features were assumed to be steady for  $\sim 3\text{--}4$  min with respect to an analysis time. Markowski et al. (2002) noted that there was confidence that such steadiness assumptions were not too severe, for the analyzed fields tended to be free of noise. This assumption of steadiness is similar to that employed for the pseudo-dual-Doppler analysis of airborne radar data. A complete discussion of the data quality control, error analysis, and the time-to-space conversion of the MM data is provided by Markowski et al. (2002).

#### d. Upper-air data

Upper-air observations were made by three mobile laboratories [Mobile Cross-Chain Loran Atmospheric Sounding System (M-CLASS; Rust et al. 1990)] operated by the National Severe Storms Laboratory (NSSL) and a fourth operated by NCAR. Prior to storm initiation and during supercell evolution, the mobile laboratories obtained soundings in the near-storm environ-

ment with launches every 120 min, and more frequently when possible.

### 3. The storm environment

#### a. Large-scale environment

A frontal boundary was oriented northeast–southwest across Kansas, becoming weak and diffuse across the eastern Oklahoma Panhandle; an east–west boundary was located south of the frontal boundary in Oklahoma and extended westward into the Oklahoma Panhandle; and a dryline extended southward through the Texas Panhandle. These boundaries passed through a low pressure system in the Texas Panhandle (Fig. 1).

In the midtroposphere, a trough was present over the western half of the country with a closed low centered over southern Nevada (Fig. 2) and a broad area of southwest flow was approaching the VORTEX experimental area. In the upper troposphere (Fig. 3), two jet streaks were rotating around the closed low. One jet was located across Utah and southwestern Wyoming;

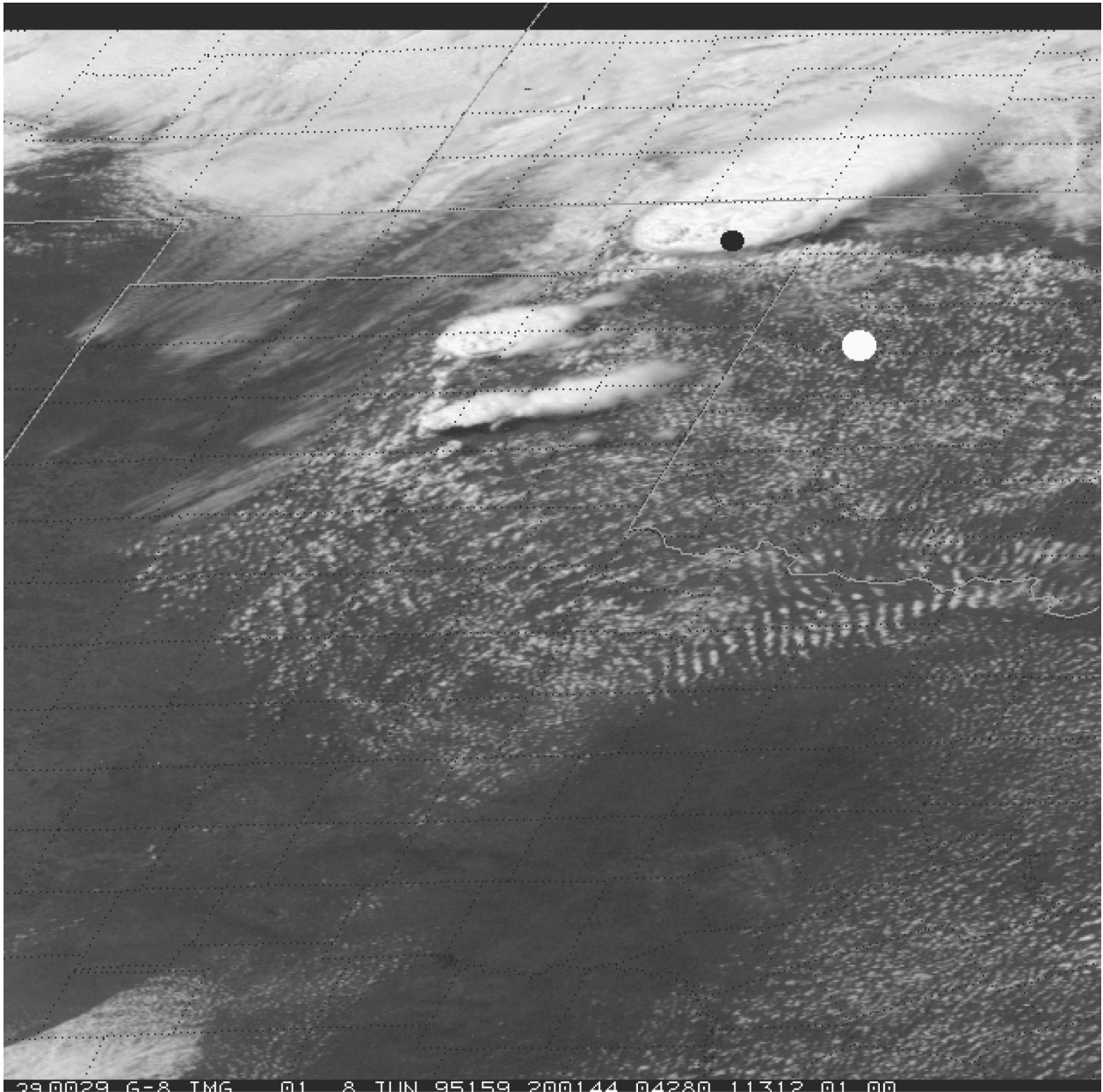


FIG. 4. GOES-8 visible imagery over the VORTEX area for 2000 UTC 8 Jun 1995. The white and black dots denote the locations of the NCAR M-CLASS launch sites at 1830 and 2030 UTC, respectively.

the second jet was located farther south and was over southern Arizona, southern New Mexico, and then turned northeastward toward the Texas Panhandle.

The Beaver County storm was the first supercell of the day and developed on the east–west boundary and just east of the intersection with the dryline at ~1845 UTC, moving northeast initially and then more to the east during its supercell phase. Additional storms developed shortly thereafter along the dryline. Figure 4 is a visible satellite image and shows the developing su-

percells in both the Oklahoma and Texas Panhandles. Also visible is a line of enhanced cumulus development in the Oklahoma Panhandle that marked the location of the surface boundary.

#### b. Near-storm environment

Rawinsonde data were analyzed from M-CLASS soundings that were launched in northwestern Oklahoma, the northeastern Texas Panhandle, and the eastern Oklahoma Panhandle at ~1800 and ~2030 UTC;

TABLE 1. Shear and instability parameters for M-CLASS soundings at 1830 and 2030 UTC. Subscripts refer to the depth in kilometers above the ground through which the calculation is performed. Values in parentheses refer to the quartile (Q) for which these numbers compare to the results presented in Rasmussen and Blanchard (1998) and Rasmussen (2003).

Parameter	NCAR 1830 UTC	NSSL-4 1830 UTC	NCAR 2030 UTC	NSSL-3 2030 UTC
SRH <sub>0-3</sub> (m <sup>2</sup> s <sup>-2</sup> )	225 (Q3)	380 (Q4)	350 (Q4)	370 (Q4)
SRH <sub>0-1</sub> (m <sup>2</sup> s <sup>-2</sup> )	110 (Q3)	135 (Q3)	15 (Q1)	85 (Q2)
CAPE (J kg <sup>-1</sup> )	3600 (Q4)	4950 (Q4)	3760 (Q4)	4900 (Q4)
CAPE <sub>0-3</sub> (J kg <sup>-1</sup> )	10 (Q1)	30 (Q2)	15 (Q1)	40 (Q2)
CIN (J kg <sup>-1</sup> )	-1 (Q1)	-29 (Q4)	-6 (Q1)	-15 (Q3)
Mean shear <sub>0-4</sub> ( $\times 10^{-3}$ s <sup>-1</sup> )	11.0 (Q4)	14.5 (Q4)	11.7 (Q4)	9.6 (Q4)
Bulk shear <sub>0.5-6</sub> (m s <sup>-1</sup> )	21 (Q3)	20 (Q3)	27 (Q4)	20 (Q3)
EHI	5.1 (Q4)	10.8 (Q4)	7.8 (Q4)	10.9 (Q4)
VGP (m s <sup>-2</sup> )	0.67 (Q4)	0.98 (Q4)	0.70 (Q4)	0.68 (Q4)

NCAR M-CLASS launch locations are shown in Fig. 4. All of the soundings indicated strong vertical wind shear and large convective buoyancy. Tabular data for the soundings are given in Table 1 and representative soundings are shown in Fig. 5.

Convective available potential energy (CAPE; Moncrieff and Miller 1976) at 1800 and 2030 UTC ranged from 3600 to 4950 J kg<sup>-1</sup>. CAPE was computed using a mixed layer of 100 hPa (often referred to as mean layer CAPE, or MLCAPE) and used the virtual temperature correction discussed by Doswell and Rasmussen (1994) and the U.S. Air Force Air Weather Service (AWS 1961). Storm-relative helicity in the 0–3-km AGL layer

(SRH<sub>0-3</sub>; Davies-Jones 1984) ranged from 225 to 380 m<sup>2</sup> s<sup>-2</sup>. These CAPE and SRH values (Table 1) were very large and compare to the third and fourth quartiles of values for tornadic supercells (Rasmussen and Blanchard 1998, hereinafter RB98).

Rasmussen (2003, hereinafter R03) also assessed the 0–1-km SRH (SRH<sub>0-1</sub>) and noted that it produced better discrimination between tornadic and nontornadic supercells than did SRH<sub>0-3</sub>. SRH<sub>0-1</sub> values ranged from 110 to 135 m<sup>2</sup> s<sup>-2</sup>. These values compare to the third quartile for tornadic supercells (R03).

Other parameters tested by RB98 and included in Table 1 are the 0–4-km mean shear, which is the length

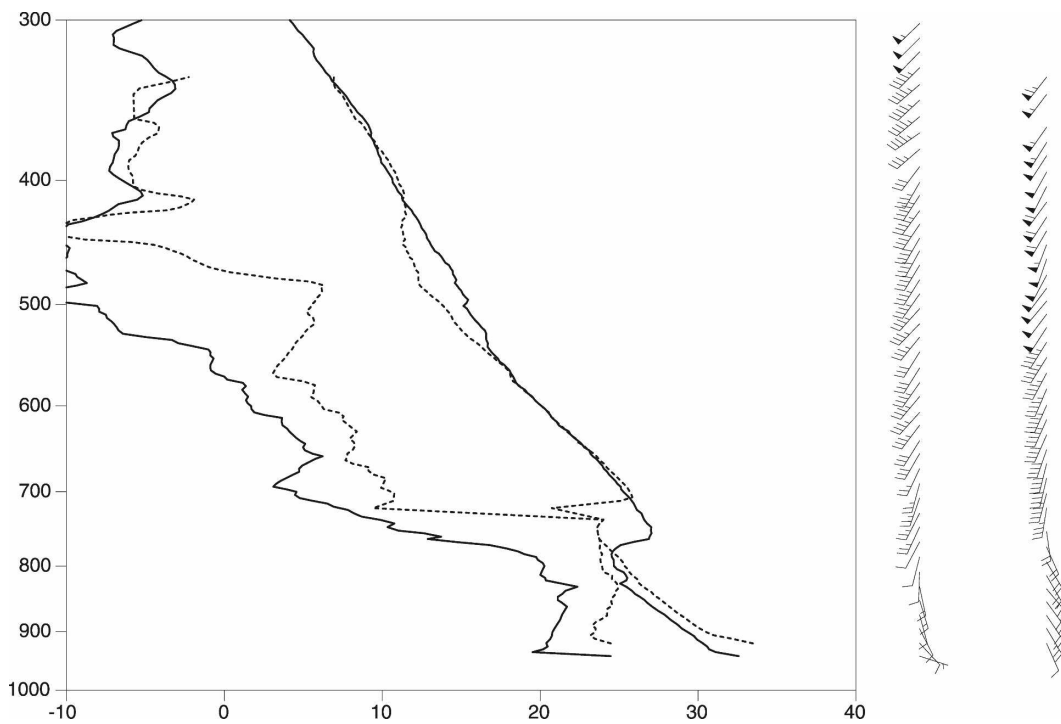


FIG. 5. Skew  $T$ -log $p$  diagram of the NCAR M-CLASS soundings. Profiles are at 1830 UTC (solid lines, and set of wind barbs on left), and 2030 UTC (dashed lines, and set of wind barbs on right). Location of the 1830 and 2030 UTC launch sites are shown in Fig. 4.

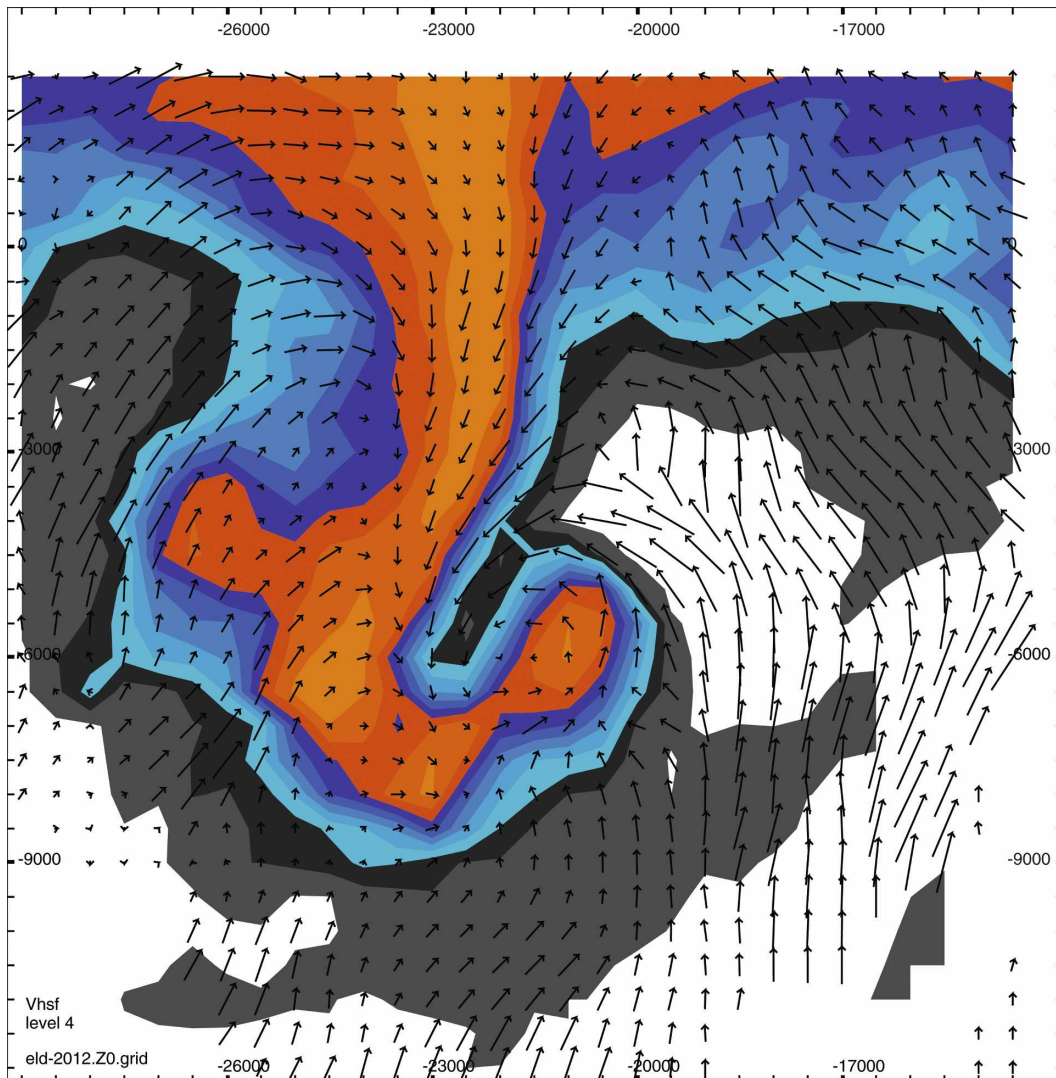


FIG. 6. Objectively analyzed reflectivity and 2D winds from the ELDORA at 2012 UTC. Height is 3500 m MSL, or approximately 2700 m AGL.

of the hodograph divided by the depth over which the hodograph was measured (Rasmussen and Wilhelmson 1983); the bulk shear from 0.5 to 6 km, which is the magnitude of the shear vector between the 0–500-m AGL mean wind and the 6-km AGL wind; the dimensionless energy helicity index (EHI; Hart and Korotky 1991; Davies 1993); the vorticity generation parameter (VGP; RB98); and convective inhibition (CIN).

All of these parameters had values that compared favorably to the results given by RB98 and R03 for supercell and tornadic storms. Thus, the near-storm environment presented an atmosphere with buoyancy and shear that was conducive to the evolution of storms into supercells and that the development of both midlevel and low-level mesocyclonic circulations was likely. In fact, this storm did develop both midlevel and low-level

circulations and these appeared to influence the behavior of the surface boundary.

#### 4. Interaction between the supercell storm and surface boundary

In this section, radar and surface data are presented to illustrate how the surface boundary responded to the development and strengthening of the low-level circulation in the supercell. Pseudo-Doppler analysis from the ELDORA will be shown to indicate the reflectivity structure and associated wind field. Base scans from the DOW are combined with MM surface observations to depict the low-level reflectivity field and the surface wind field. Last, surface plots and meteograms using the Oklahoma Mesonet are presented to show how the

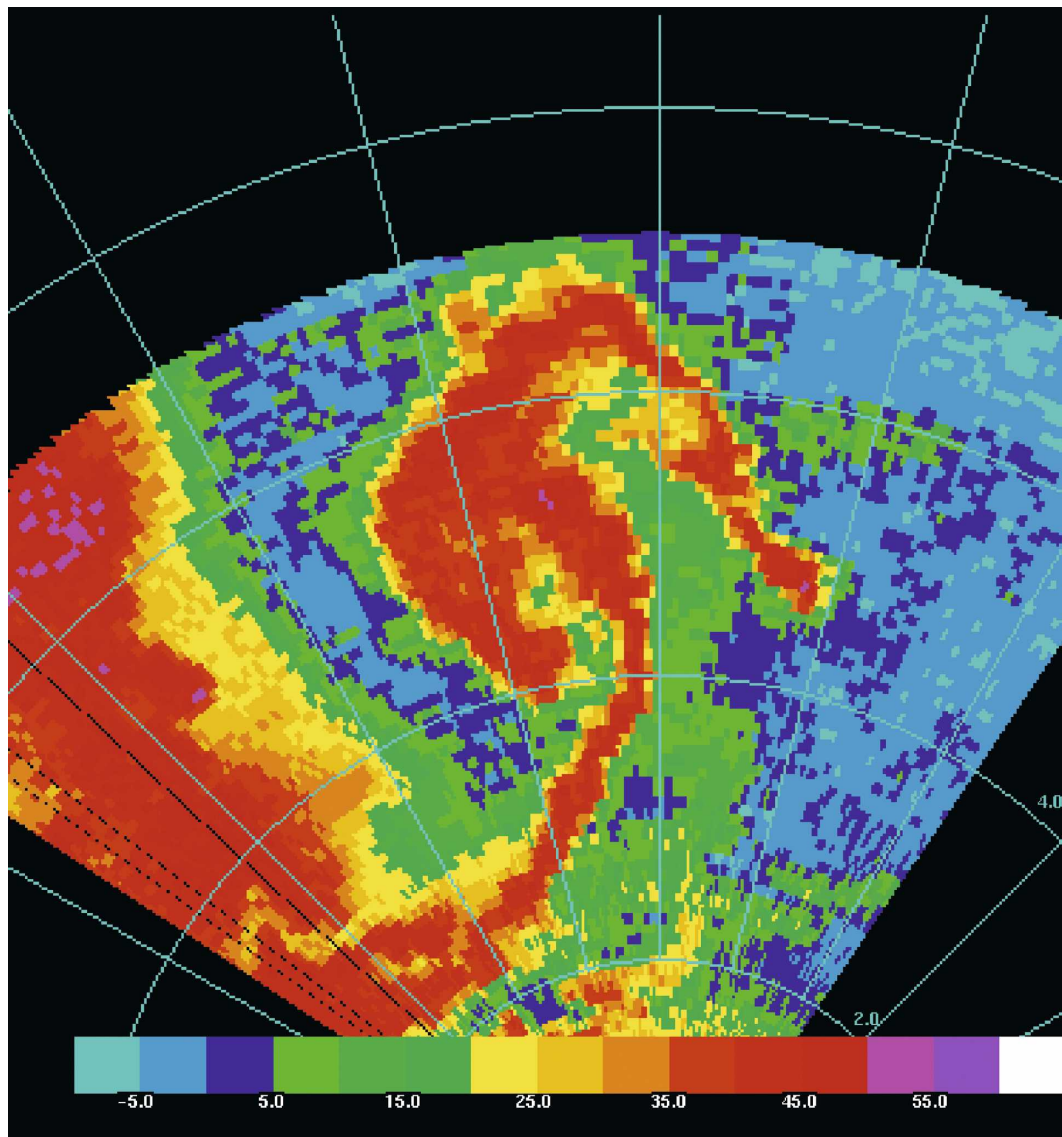


FIG. 7. Reflectivity at 1.1° elevation scan from the DOW at 2016 UTC 8 Jun 1995. Range rings are drawn every 2 km.

northward advance and subsequent southward retreat of the boundary was captured with these data.<sup>1</sup>

Airborne Doppler data were available from the ELDORA for the period 1950–2012 UTC—a period in which the storm was a supercell with a deep, strong,

<sup>1</sup> It should be recognized that the frontal boundary is three dimensional. Although it is desirable to assess and discuss the three dimensionality of this feature, it is not possible. Neither the NCAR ELDORA nor the NOAA P-3 aircraft flew transects across the boundary. Instead, they were flying “racetrack” patterns on the inflow side of the storm north of the surface boundary. As a consequence, the three-dimensional structure cannot be known. There are only the 5-min data from the Oklahoma Mesonet to track the surface location of the boundary.

persistent mesocyclone. This feature is best illustrated in Fig. 6, a pseudo-Doppler analysis of the low-level wind field superimposed upon the storm reflectivity. This analysis shows the well-developed low-level circulation associated with the supercell storm.

DOW radar data at 2016 UTC (Fig. 7) showed a tornado-like signature (Wurman and Gill 2000; Bluestein and Pazmany 2000; Bluestein et al. 2003, 2004; Alexander and Wurman 2005) in the reflectivity field (i.e., a cyclonically banded structure). Velocities at the base tilt ( $\sim 85$  m AGL) showed a differential velocity of  $20 \text{ m s}^{-1}$ , although this low-level circulation did not produce a visible dust swirl or any other visible near-ground manifestation, based on reports from the

TABLE 2. Gate-to-gate and mesocyclone  $\Delta V$  detected by the DOW at 2025 UTC at various tilts and elevations above the ground.

Scan	Height above ground (m)	Gate-to-gate $\Delta V$ ( $\text{m s}^{-1}$ )	Mesocyclone $\Delta V$ ( $\text{m s}^{-1}$ )
S0 (1.1°)	85	16	32
S1 (2.0°)	155	31	63
S2 (4.0°)	350	47	64
S3 (6.1°)	530	30	51
S4 (7.9°)	650	30	59
S5 (10.1°)	870	30	48

numerous VORTEX crews operating in the area (Blanchard and Straka 1998).

During the period 2020–2036 UTC, the DOW continued to show a low-level circulation. The differential velocity near the tip of the hook echo was  $\sim 20\text{--}30 \text{ m s}^{-1}$  and was observable at the base tilt. The DOW also observed a strong, deep, midlevel mesocyclone with differential velocities of  $32\text{--}64 \text{ m s}^{-1}$  and gate-to-gate differential velocities of  $16\text{--}47 \text{ m s}^{-1}$  (Table 2). The mesocyclone was  $\sim 8\text{--}10 \text{ km}$  in diameter; a stronger embedded circulation of  $\sim 2\text{--}3 \text{ km}$  in diameter may be the tornado vortex signature (Brown et al. 1978). In addition, during this period the MM data indicated that there was a circulation at the surface and that this circulation was located near the tip of the radar-observed hook echo.

An analysis of high spatial and temporal resolution Oklahoma Mesonet data (Brock et al. 1995) suggested that the circulation associated with the mesocyclone might have been responsible for drawing the frontal boundary northward and to become associated with the supercell (Fig. 8). Note that the temperature increased at the Slapout, Oklahoma, station (abbreviated SLAP) located just north of the northeast corner of the Texas Panhandle, and the wind veered from northeast to south as the front moved northward toward the supercell in Beaver County. It is also clear from Fig. 8 that the storm is moving to the northeast and away from the boundary and that any reduction in distance between the supercell and the boundary must be attributed to the northward motion of the boundary rather than any southward motion or propagation of the supercell.

A meteogram of SLAP (Fig. 9) shows the changes in temperature, dewpoint, and wind as the front moves northward across the station. A composite of DOW radar data and MM data (Fig. 10) showed that the mesocyclone was creating a supercell-scale occlusion with the warm sector located only a short distance to the south.

Inspection of the temperature, dewpoint, and wind in the warm sector shows that these values were essentially the same as those found to the south of the east-

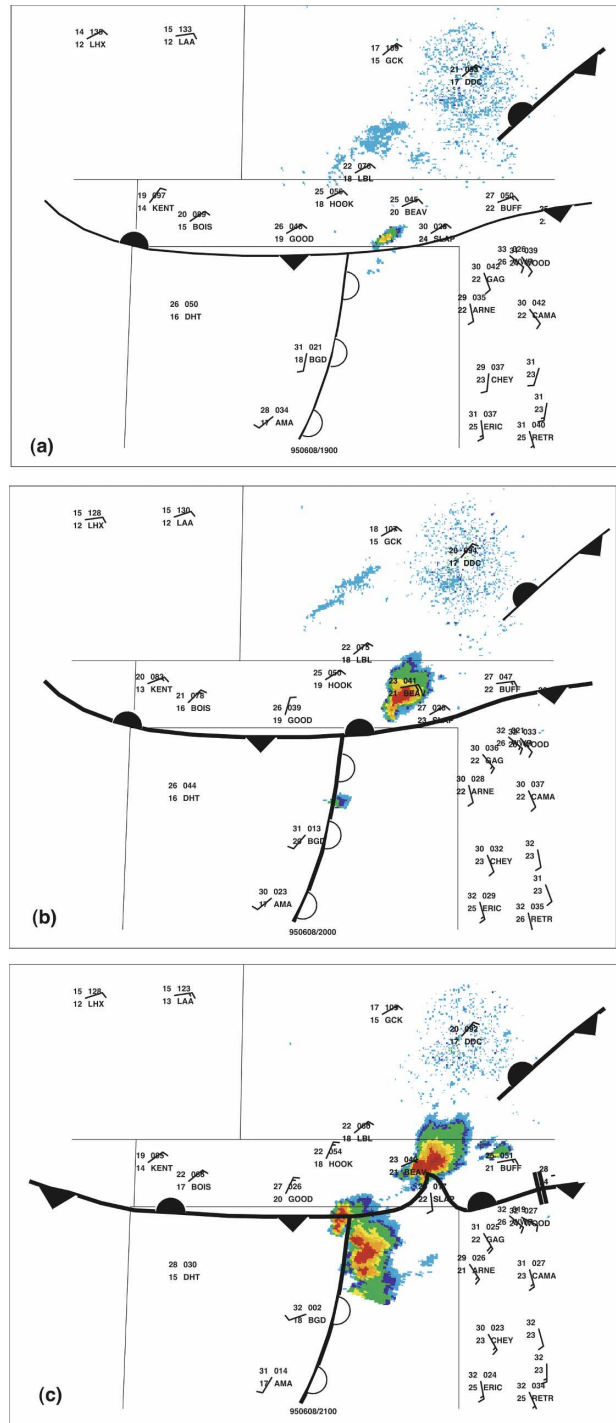


FIG. 8. Base scan reflectivity from the WSR-88D at Dodge City, KS, (station abbreviation KDDC) overlain with surface data and surface boundaries at (top) 1900, (middle) 2000, and (bottom) 2100 UTC. Station plots are as in Fig. 1, but with the station abbreviation included at the lower right.

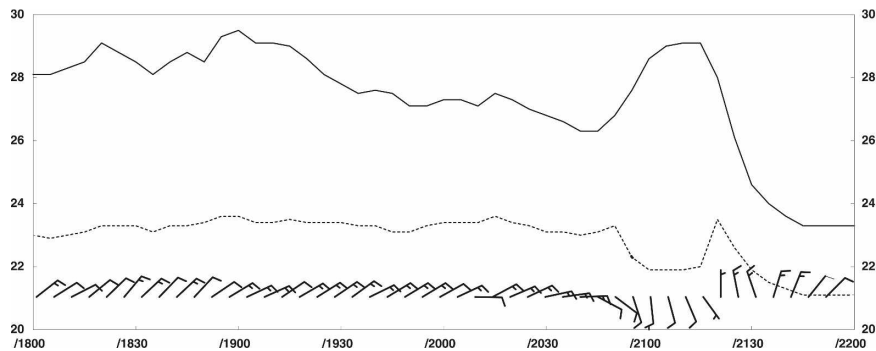


FIG. 9. Surface meteorogram for station SLAP for the period 1800–2200 UTC 8 Jun 1995 (the horizontal scale indicates 30-min increments). Curves are temperature (solid top line) and dewpoint (bottom dotted line) in degrees Celsius (the vertical scale extends from 20° to 30°C in 2°C increments). Wind barbs (below dotted line) are in meters per second, with a full barb at 5 m s<sup>-1</sup> and a half barb at 2.5 m s<sup>-1</sup>.

west boundary shown in Fig. 1, indicating that the boundary shown here is probably the same boundary that was located farther south at an earlier time. Thus, we have reasonable evidence that the boundary was significantly influenced by the low-level wind field and circulation associated with the mesocyclonic supercell.

This is interesting for at least one reason: recent work has suggested that a supercell is more likely to become tornadic if it remains near a surface boundary in which low-level horizontal vorticity associated with the boundary is available for tilting into the vertical direction. The Beaver County storm suggests one possible mechanism in which a supercell may remain in proximity to a favorable boundary.

Although the supercell remained in proximity to the boundary for an extended period, the storm never produced a tornado. Previous analyses of this event have portrayed this storm as an example of tornadogenesis failure (Blanchard and Straka 1998; Markowski et al. 2002).

## 5. Discussion

The previous section presented the evolution of the boundary and how it was drawn northward and was briefly entrained into the low-level circulation of the supercell passing over Beaver County, Oklahoma. The literature contains many examples of the interaction between supercell thunderstorms and boundaries, including thunderstorm outflows boundaries and frontal boundaries.

Early operational forecasting papers by Magor (1959) and Miller (1967) emphasized the importance of this frequently observed phenomenon. Satellite analyses of Purdom (1976) showed increases in thunderstorm intensity for individual storms as they moved across or along such boundaries.

Maddox et al. (1980) were motivated by these earlier papers and examined the interaction of convective storms with baroclinic zones including warm fronts, stationary fronts, or old, slow-moving thunderstorm outflow boundaries. Their results clearly showed that storms intensified and were more likely to be tornadic in proximity to these thermal boundaries. None of their cases, however, showed a boundary being drawn into the mesocirculation; rather, the storms were shown to approach and cross the boundaries with no response by the boundary to the storm. It is possible, however, that some of these storms may have influenced the boundary, but the data used in their study were too coarse to make these detailed observations.

Markowski et al. (1998) examined the occurrence of tornadoes in supercells interacting with boundaries from the cases collected during VORTEX (Rasmussen et al. 1994). They reiterated that a number of past studies have presented evidence that low-level boundaries were associated with tornadic supercells. They found that nearly 70% of the tornadoes observed in VORTEX were associated with identifiable, preexisting boundaries (i.e., this excludes the boundaries generated by both rear- and forward-flank downdrafts of the parent storm). Note that their Table 1 includes 8 June 1995 storms in the eastern Texas Panhandle but does not include the Beaver County storm since it was a tornadogenesis failure.

They additionally noted that storms that moved along a boundary rather than directly across may have better chances of processing both unstable air and larger horizontal vorticity in the vicinity of the boundary. As with Maddox et al. (1980), however, they did not comment on whether any of these boundary-crossing storms significantly modified the boundary.

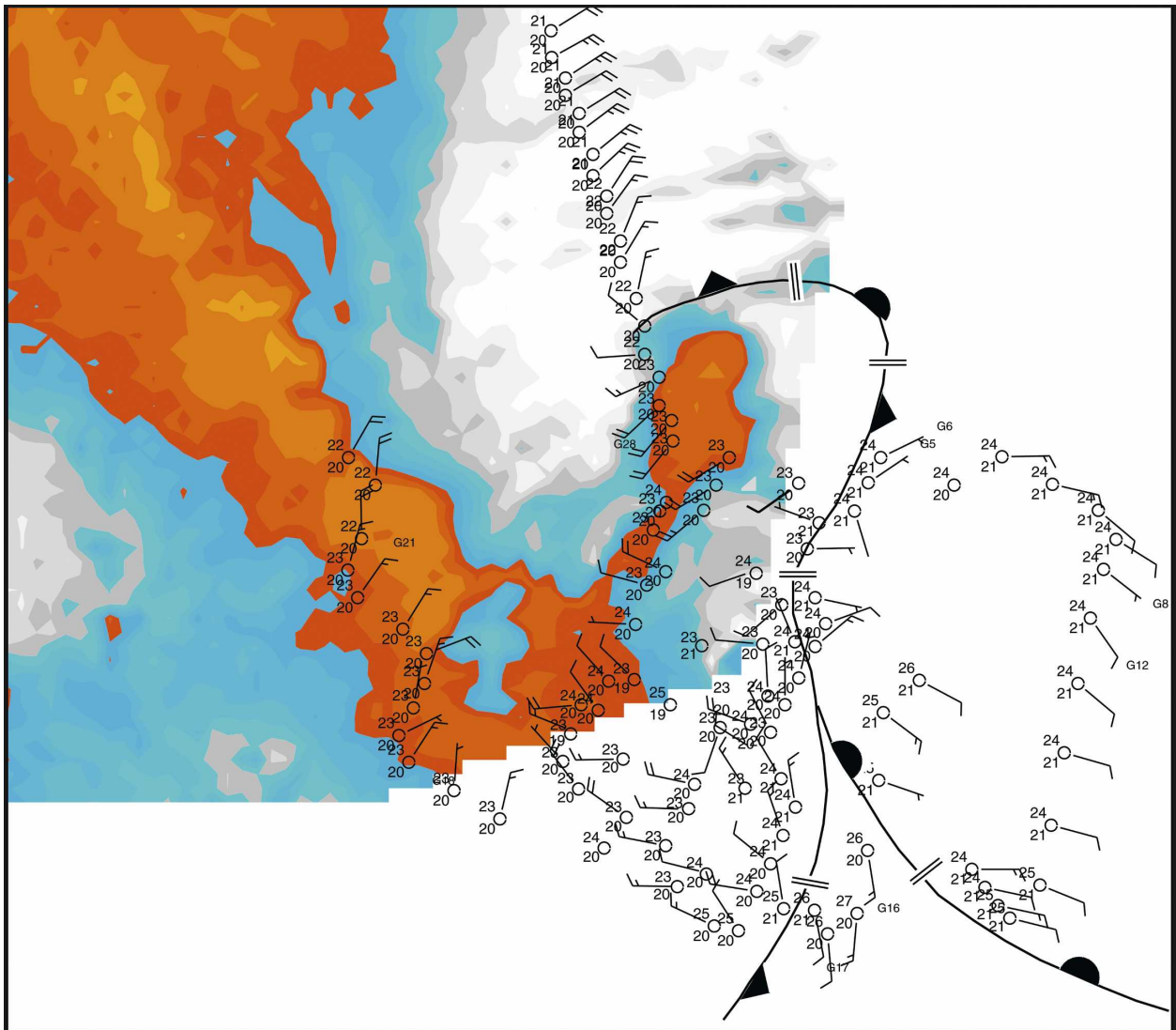


FIG. 10. Base scan reflectivity from the DOW with MM surface observations overlain at 19 UTC 8 Jun 1995; the MM observations have been selectively thinned for legibility.

Dostalek et al. (2004) discussed a tornadic left-moving member of a splitting supercell that traveled northward and remained in proximity to the northward-moving outflow boundary associated with the initial storm.

Weaver and Nelson (1982) examined a tornadic supercell and its interaction with outflow boundaries. They noted that instead of the outflow boundary racing out ahead of the storm to cut off the inflow it remained quasi-steady with respect to the storm and was drawn back into the storm near the mesocirculation; that is, the gust front cloud had “wrapped back” into the storm. Note that the storm and the leading edge of the outflow were moving in the same general direction. Although there are some similarities between the current study

and those of both Weaver and Nelson (1982) and Dostalek et al. (2004), there is one important difference: in the current case, the storm moved away from the boundary and yet the supercell circulation was sufficient to draw the boundary back into proximity.

It consequently appears that this event and case study depict an evolution and interaction not previously recognized or documented. It is likely, however, that there have been other events that behaved in a similar manner but have not been captured in a data-rich environment.

*Acknowledgments.* The author extends his appreciation to the many scientists and students who participated in VORTEX and collected extraordinary

datasets; to the joint efforts of NCAR, OU, and NSSL and J. Wurman for the development and deployment of the Doppler on Wheels radar; to J. Straka for his significant efforts in editing the DOW velocity data; and to E. Rasmussen for his scientific vision and support. Portions of this research were supported by National Science Foundation Grants ATM-9617318 and ATM-9120009 while the author was affiliated with the National Severe Storms Laboratory and the Cooperative Institute for Mesoscale Meteorological Studies, University of Oklahoma.

## REFERENCES

- Alexander, C. R., and J. Wurman, 2005: The 30 May 1998 Spencer, South Dakota, storm. Part I: The structural evolution and environment of the tornadoes. *Mon. Wea. Rev.*, **133**, 72–97.
- AWS, 1961: Use of the skew  $T$ , log  $p$  diagram in analysis and forecasting. Vol. 1. AWSM 105-124, 144 pp. [Available from Headquarters, Air Force Weather Agency, Scott AFB, IL 62225.]
- Blanchard, D. O., and J. M. Straka, 1998: Some possible mechanisms for tornadogenesis failure in a supercell. Preprints, *19th Conf. on Severe Local Storms*, Minneapolis, MN, Amer. Meteor. Soc., 116–119.
- Bluestein, H. B., and A. L. Pazmany, 2000: Observations of tornadoes and other convective phenomena with a mobile, 3-mm wavelength, Doppler radar. *Bull. Amer. Meteor. Soc.*, **81**, 2939–2952.
- , C. C. Weiss, and A. L. Pazmany, 2003: Mobile Doppler radar observations of a tornado in a supercell near Bassett, Nebraska, on 5 June 1999. Part I: Tornadogenesis. *Mon. Wea. Rev.*, **131**, 2954–2967.
- , —, and —, 2004: The vertical structure of a tornado near Happy, Texas, on 5 May 2002: High-resolution, mobile, W-band, Doppler-radar observations. *Mon. Wea. Rev.*, **132**, 2325–2337.
- Brock, F. V., K. C. Crawford, R. L. Elliott, G. W. Cuperus, S. J. Stadler, H. L. Johnson, and M. D. Eilts, 1995: The Oklahoma Mesonet: A technical overview. *J. Atmos. Oceanic Technol.*, **12**, 5–19.
- Brown, R. A., L. R. Lemon, and D. W. Burgess, 1978: Tornado detection by pulsed Doppler radar. *Mon. Wea. Rev.*, **106**, 29–38.
- Davies, J. M., 1993: Hourly helicity, instability, and EHI in forecasting supercell tornadoes. Preprints, *17th Conf. on Severe Local Storms*, St. Louis, MO, Amer. Meteor. Soc., 107–111.
- Davies-Jones, R. P., 1984: Streamwise vorticity: The origin of updraft rotation in supercell storms. *J. Atmos. Sci.*, **41**, 2991–3006.
- Dostalek, J. F., J. F. Weaver, and G. L. Phillips, 2004: Aspects of a tornadic left-moving thunderstorm of 25 May 1999. *Wea. Forecasting*, **19**, 614–626.
- Doswell, C. A., III, and E. N. Rasmussen, 1994: The effect of neglecting the virtual temperature correction on CAPE calculations. *Wea. Forecasting*, **9**, 625–629.
- Hart, J. A., and W. Korotky, 1991: The SHARP workstation v1.50 users guide. NOAA/National Weather Service, 30 pp. [Available from NWS Eastern Region Headquarters, 630 Johnson Ave., Bohemia, NY 11716.]
- Hildebrand, P. H., and Coauthors, 1996: The ELDORA/ASTRAIA airborne Doppler weather radar: High-resolution observations from TOGA COARE. *Bull. Amer. Meteor. Soc.*, **77**, 213–232.
- Maddox, R. A., L. R. Hoxit, and C. F. Chappell, 1980: A study of tornadic thunderstorm interaction with thermal boundaries. *Mon. Wea. Rev.*, **108**, 322–336.
- Magor, B. W., 1959: Mesoanalysis: Some operational analysis techniques utilized in tornado forecasting. *Bull. Amer. Meteor. Soc.*, **40**, 499–511.
- Markowski, P. M., E. N. Rasmussen, and J. M. Straka, 1998: The occurrence of tornadoes in supercells interacting with boundaries during VORTEX-95. *Wea. Forecasting*, **13**, 852–859.
- , J. M. Straka, and E. N. Rasmussen, 2002: Direct surface thermodynamic observations within the rear-flank downdrafts of nontornadic and tornadic supercells. *Mon. Wea. Rev.*, **130**, 1692–1721.
- Miller, R. C., 1967: Notes on analysis and severe-storm forecasting procedures of the Military Weather Warning Center. AWS Tech. Rep. 200, 94 pp. [Available from Headquarters, Air Force Weather Agency, Scott AFB, IL 62225.]
- Moncrieff, M. W., and M. J. Miller, 1976: The dynamics and simulation of tropical cumulonimbus and squall lines. *Quart. J. Roy. Meteor. Soc.*, **102**, 373–394.
- Purdum, J. F. W., 1976: Some uses of high-resolution GOES imagery in the mesoscale forecasting of convection and its behavior. *Mon. Wea. Rev.*, **104**, 1474–1483.
- Rasmussen, E. N., 2003: Refined supercell and tornado parameters. *Wea. Forecasting*, **18**, 530–535.
- , and R. B. Wilhelmson, 1983: Relationships between storm characteristics and 1200 GMT hodographs, low-level shear, and stability. Preprints, *13th Conf. on Severe Local Storms*, Tulsa, OK, Amer. Meteor. Soc., J5–J8.
- , and D. O. Blanchard, 1998: A baseline climatology of sounding-derived supercell and tornado forecast parameters. *Wea. Forecasting*, **13**, 1148–1164.
- , J. M. Straka, R. P. Davies-Jones, C. A. Doswell, F. Carr, M. Eilts, and D. R. MacGorman, 1994: Verification of the Origins of Rotation in Tornadoes Experiment: VORTEX. *Bull. Amer. Meteor. Soc.*, **75**, 995–1006.
- , S. Richardson, J. M. Straka, and D. O. Blanchard, 2000: The association of significant tornadoes with a baroclinic boundary on 2 June 1995. *Mon. Wea. Rev.*, **128**, 174–191.
- Rust, W. D., R. P. Davies-Jones, D. W. Burgess, R. A. Maddox, L. C. Showell, T. C. Marshall, and D. K. Lauritsen, 1990: Testing a mobile version of a cross-chain loran atmospheric sounding system (M-CLASS). *Bull. Amer. Meteor. Soc.*, **71**, 173–180.
- Straka, J. M., E. N. Rasmussen, and S. E. Fredrickson, 1996: A mobile mesonet for finescale meteorological observations. *J. Atmos. Oceanic Technol.*, **13**, 921–936.
- Wakimoto, R. M., W.-C. Lee, H. B. Bluestein, C.-W. Liu, and P. H. Hildebrand, 1996: ELDORA observations during VORTEX 95. *Bull. Amer. Meteor. Soc.*, **77**, 1465–1482.
- Weaver, J. F., and S. P. Nelson, 1982: Multiscale aspects of thunderstorm gust fronts and their effects on subsequent storm development. *Mon. Wea. Rev.*, **110**, 707–718.
- Wurman, J., and S. Gill, 2000: Finescale radar observations of the Dimmitt, Texas (2 June 1995), tornado. *Mon. Wea. Rev.*, **128**, 2135–2165.
- , J. M. Straka, E. N. Rasmussen, M. Randall, and A. Zahrai, 1997: Design and deployment of a portable, pencil-beam, pulsed, 3-cm Doppler radar. *J. Atmos. Oceanic Technol.*, **14**, 1502–1512.
- Young, G. S., and J. M. Fritsch, 1989: A proposal for general conventions in analyses of mesoscale boundaries. *Bull. Amer. Meteor. Soc.*, **70**, 1412–1421.